Available online at www.sciencedirect.com

ScienceDirect

Geochimica et Cosmochimica Acta 144 (2014) 25–42

Geochimica et Cosmochimica Acta

www.elsevier.com/locate/gca

Controls on thallium uptake during hydrothermal alteration of the upper ocean crust

Rosalind M. Coggon [a,*], Mark Rehkämper [a], Charlotte Atteck [a], Damon A.H. Teagle [b], Jeffrey C. Alt [c], Matthew J. Cooper [b]

[a] *Department of Earth Science and Engineering, South Kensington Campus, Imperial College London, London SW7 2AZ, UK*

[b] *Ocean and Earth Science, National Oceanography Centre Southampton, University of Southampton, European Way, Southampton SO14 3ZH, UK*

[c] *Earth and Environmental Sciences, University of Michigan, 2534 C.C. Little Building, 1100 North University Ave, Ann Arbor, MI 48109-1005, USA*

Received 26 November 2013; accepted in revised form 1 September 2014; available online 16 September 2014

Abstract

Hydrothermal circulation is a fundamental component of global biogeochemical cycles. However, the magnitude of the high temperature axial hydrothermal fluid flux remains disputed, and the lower temperature ridge flank fluid flux is difficult to quantify. Thallium (Tl) isotopes behave differently in axial compared to ridge flank systems, with Tl near-quantitatively stripped from the intrusive crust by high temperature hydrothermal reactions, but added to the lavas during low temperature reaction with seawater. This contrasting behavior provides a unique approach to determine the fluid fluxes associated with axial and ridge flank environments. Unfortunately, our understanding of the Tl isotopic mass balance is hindered by poor knowledge of the mineralogical, physical and chemical controls on Tl-uptake by the ocean crust.

Here we use analyses of basaltic volcanic upper crust from Integrated Ocean Drilling Program Hole U1301B on the Juan de Fuca Ridge flank, combined with published analyses of dredged seafloor basalts and upper crustal basalts from Holes 504B and 896A, to investigate the controls on Tl-uptake by mid-ocean ridge basalts and evaluate when in the evolution of the ridge flank hydrothermal system Tl-uptake occurs.

Seafloor basalts indicate an association between basaltic uptake of Tl from cold seawater and uptake of Cs and Rb, which are known to partition into K-rich phases. Although there is no clear relationship between Tl and K contents of seafloor basalts, the data do not rule out the incorporation of at least some Tl into the same minerals as the alkali elements. In contrast, we find no relationship between the Tl content and either the abundance of secondary phyllosilicate minerals, or the K, Cs or Rb contents in upper crustal basalts. We conclude that the uptake of Tl and alkali elements during hydrothermal alteration of the upper crust involves different processes and/or mineral phases compared to those that govern seafloor weathering. Furthermore, a correlation between the Tl and S concentrations of upper crustal basalts from Holes U1301B, 504B and 896A indicates that Tl is primarily incorporated into secondary sulfides. Given that some of these secondary sulfides formed as a result of microbial sulfate reduction, microbial action is at least indirectly responsible for Tl-uptake.

Thallium-enrichment of ridge flank basalts requires a Tl-bearing fluid and physical, chemical and microbial conditions that favor secondary sulfide formation. Uptake of Tl occurs in reducing environments in the background rocks away from fluid

* Corresponding author at: Ocean and Earth Science, National Oceanography Centre Southampton, University of Southampton, European Way, Southampton SO14 3ZH, UK. Tel.: +44 023 8059 6539.

E-mail addresses: R.M.Coggon@soton.ac.uk (R.M. Coggon), markrehk@imperial.ac.uk (M. Rehkämper), Damon.Teagle@southampton.ac.uk (D.A.H. Teagle), jalt@umich.edu (J.C. Alt), matthew.cooper@noc.soton.ac.uk (M.J. Cooper).

http://dx.doi.org/10.1016/j.gca.2014.09.001

flow pathways during early 'open' circulation of oxidizing seawater but more pervasively throughout the system during later 'restricted' circulation of reducing fluids. The Tl-isotope system is therefore a useful tracer of the fluid flux through both the 'open' and 'restricted' ridge flank hydrothermal regimes.

1. INTRODUCTION

The production of ocean crust during mid-ocean ridge magmatism is a key component of the plate tectonic cycle and the principal mechanism of heat loss from the Earth's interior. Approximately one third of the heat lost through the ocean crust is removed by thermally driven circulation of seawater-derived fluids through the ocean crust. Hydrothermal circulation influences the geometry and distribution of magma chambers at the mid-ocean ridges as well as the chemistry and physical properties (e.g., porosity, permeability, and seismic velocities) of the ocean crust (Alt, 1995). Hydrothermal fluids react with the crust resulting in the precipitation of secondary minerals, modifying the chemistry of both the fluid and the rock. Consequently hydrothermal circulation is a fundamental component of global geochemical cycles, with the venting of buoyant hydrothermal fluids through the seafloor having a profound effect on the composition of the oceans and atmosphere, whereas subduction of altered ocean crust affects the chemistry of the upper mantle and new crust formed in arcs. Hydrothermal contributions to the oceans influence many of the paleoceanographic records (e.g., Sr, S or O) we use to reconstruct past climate (Zachos et al., 2001; Lear et al., 2002), weathering (Vance et al., 2009) or other Earth events (Prokoph and Veizer, 1999; Veizer et al., 1999). Reliable estimates of the thermal, fluid and chemical fluxes associated with hydrothermal circulation are therefore crucial to our understanding of the formation of ocean crust and the evolution of our planet.

Axial magma chambers power high temperature (up to ~400 °C) hydrothermal systems that vent at the seafloor through 'black-smoker' sulfide chimneys and support unique chemosynthetic ecosystems. However, two thirds of global hydrothermal heat loss occurs on the ridge flanks, where circulation persists for tens of millions of years, driven by conductive cooling of the oceanic lithosphere (Stein and Stein, 1994). Since more heat is removed from the ridge flanks by fluids at lower temperatures (<100 °C) than in axial black-smoker systems, the fluid flux through the ridge flanks is necessarily several orders of magnitude greater (Mottl, 2003). Consequently, even small modifications to the fluid chemistry may result in significant chemical fluxes to the oceans, particularly for elements such as Mg, for which fluid–rock exchange can occur at low temperatures (Mottl and Wheat, 1994). In principle, isotope and element abundance data for hydrothermal fluids and altered ocean crust can be used to obtain independent geochemical estimates of hydrothermal fluid fluxes, either: (i) through balancing global ocean chemical budgets or (ii) by determining the fluid flux required to produce an observed shift in ocean crust composition due to fluid–rock exchange, given measured vent fluid compositions. To better quantify the axial and ridge flank hydrothermal fluid and elemental fluxes we require chemical or isotopic tracers that are insensitive to the variations in riverine inputs and that can clearly distinguish between fluid exchange occurring at high and low temperatures.

Thallium (Tl) displays different behavior during low- and high-temperature hydrothermal alteration, with isotopically light Tl added to the volcanic upper crust from seawater during low temperature (<100 °C) hydrothermal alteration, whereas Tl is leached from the underlying sheeted dikes during higher temperature (>250–300 °C) hydrothermal reactions and returned to the oceans by black-smoker vent fluids (Nielsen et al., 2006b). The contrasting behavior of Tl during low- and high-temperature hydrothermal alteration was exploited to estimate the fluid fluxes associated with both portions of the hydrothermal system, using simple mass balance models (Nielsen et al., 2006b). However, the physical, chemical and mineralogical controls on Tl behavior during hydrothermal alteration remain poorly understood, primarily due to the limited analyses of ocean crust samples. Here we investigate the physical, chemical and mineralogical controls on Tl-enrichment of upper crustal basalts from the Juan de Fuca Ridge to determine the conditions and timing of Tl-uptake during low-temperature hydrothermal alteration of the upper ocean crust and evaluate when in the evolution of the hydrothermal system Tl-uptake occurs.

2. THALLIUM GEOCHEMISTRY

Thallium is a highly incompatible and volatile trace element that displays diverse behavior depending on the nature of the geochemical system (Shaw, 1952; Wedepohl, 1974). It occurs in two valence states, Tl^{+} and Tl^{3+}. The Tl^{3+} cation is only stable under strongly oxidizing conditions and hence is only relevant near the Earth's surface and in aqueous systems. Due to its small size (ionic radius = 1.0 Å; (Shannon, 1976)) and charge, Tl^{3+} is expected to exhibit geochemical behavior akin to Al^{3+} and, possibly, the trivalent rare earth elements (Rehkämper and Nielsen, 2004). Under the more reducing conditions of the silicate Earth, only Tl^{+} will be present (Rehkämper and Nielsen, 2004). The larger univalent Tl^{+} cation is of similar size and charge to the heavier alkali metals (K, Rb, and Cs) (Goldschmidt, 1954) and therefore can substitute into the K^{+} lattice sites of some silicate minerals, for example micas and K-feldspar (Shaw, 1952; Albuquerque et al., 1972; Heinrichs et al., 1980). Thallium concentrations correlate with Rb and Cs in magmatic systems, in which it displays highly incompatible, lithophile behavior (Heinrichs et al., 1980; Nielsen et al., 2006a;

Baker et al., 2010). However, Tl^+ has a more polarizable electron shell and hence is more conducive to covalent bonding than the alkali metals, and can therefore also be incorporated into sulfide minerals. Such behavior has been documented in aqueous systems (Xiao et al., 2004) and experimental evidence indicates that Tl is also slightly to moderately chalcophile during mantle melting (Wood et al., 2008; Kiseeva and Wood, 2013). On the basis of experiments, Tl is expected to display a partition coefficient between liquid sulfides and basaltic melt ($D_{sulph-melt}$) of about 15 at conditions relevant for the production of mid-ocean ridge basalts (MORB) (Kiseeva and Wood, 2013). However, the melting parameters and mineral–melt partition coefficients (Kiseeva and Wood, 2013), imply that the behavior of Tl during mantle melting is only marginally altered by the presence (or absence) of sulfides, due to the combined effects of a relatively low $D_{sulph-melt}$ value and the low mantle abundance of S (~250 ppm) and hence sulfide minerals.

In the oceans, Tl generally displays a conservative distribution and it is cycled through the marine system in a similar manner to K^+, consistent with its occurrence in the univalent state. Thallium, however, has a much shorter marine residence time (~20 ky) compared to the alkali elements (~4.5 My and 0.6–0.9 My for K and Rb, respectively) because it is scavenged by ferromanganese oxyhydroxides (Rehkämper et al., 2002; Rehkämper and Nielsen, 2004). The uptake of Tl^+ from seawater by ferromanganese minerals occurs via the formation of surface sorption complexes, with or without oxidation depending on the mineralogy of the ferromanganese deposit (Peacock and Moon, 2012; Nielsen et al., 2013).

Thallium has two naturally occurring stable isotopes, with mass numbers 203 and 205, and its isotopic composition is reported using an ε-notation, where $\varepsilon^{205}Tl$ is defined as the deviation of the $^{205}Tl/^{203}Tl$ isotope ratio of a sample from that of the NIST SRM 997 Tl isotope standard in parts per 10,000:

$$\varepsilon^{205}Tl = 10,000\left[\frac{(^{205}Tl/^{203}Tl)_{sample} - (^{205}Tl/^{203}Tl)_{SRM\ 997}}{(^{205}Tl/^{203}Tl)_{SRM\ 997}}\right] \quad (1)$$

Particularly large Tl isotope variations are observed in the marine environment, with $\varepsilon^{205}Tl$ varying between about −15 for altered oceanic basalts (Nielsen et al., 2006b) and +15 for ferromanganese crusts (Rehkämper and Nielsen, 2004; Rehkämper et al., 2002; Nielsen et al., 2009).

2.1. Thallium in mid-ocean ridge basalts

The Tl concentration of fresh MORB was previously inferred to be 3.0 ± 1.5 ng/g (Nielsen et al., 2006b). A recently published database of trace element analyses of ocean floor basaltic glasses that includes 495 extrusive mid-ocean ridge basalt glasses, indicates that fresh MORB Tl concentrations span a greater range from <1 to 45 ng/g (Jenner and O'Neill, 2012). However, the distribution of this data is skewed with 90% of the data falling within the range of 1–30 ng/g, and a median Tl concentration of 9 ng/g with an interquartile range of 7 ng/g. We therefore assume that fresh MORB has a Tl content of 1–30 ng/g, coupled with an average isotope composition of $\varepsilon^{205}Tl \approx -2.0 \pm 0.5$ (Nielsen et al., 2006a,b, 2007).

Ocean Drilling Program (ODP) Hole 504B, located in 6.9 Ma crust produced at the intermediate spreading rate Costa Rica Rift, penetrates ~600 m of volcanic lavas and ~1.2 km into the underlying sheeted dikes (Alt et al., 1996b). The volcanic section is enriched in isotopically light Tl relative to fresh MORB. There is a systematic decrease in the extent of enrichment and isotope fractionation with depth, from 250 ng/g and $\varepsilon^{205}Tl \approx -15$ at 100 meters sub-basement (msb), to fresh MORB values between ~350 and 650 msb. The Tl enrichment is attributed to secondary mineral uptake of isotopically light Tl from low-temperature (<150 °C) fluids. In contrast, the underlying sheeted dikes (700–1900 msb) have Tl isotopic compositions similar to fresh MORB but very low Tl concentrations. High temperature axial vent fluids are enriched in Tl by approximately two orders of magnitude relative to seawater (with 65 pmol/kg Tl). The Tl isotopic composition of modern vent fluids ($\varepsilon^{205}Tl \approx -1.9 \pm 0.6$) is distinct from that of seawater ($\varepsilon^{205}Tl \approx -6$) but identical to the composition of fresh MORB and the dikes. This indicates that the Tl of the vent fluids was leached from the sheeted dikes during high-temperature alteration without associated isotope fractionation (Nielsen et al., 2006b).

3. STUDY SITE

3.1. The Juan de Fuca Ridge

The Juan de Fuca Ridge (JdFR) produces ocean crust at ~6 cm/y (full rate) in the Cascadia Basin, west of North America (Fig. 1). Following its eruption, the uppermost volcanic crust is rapidly cooled to ambient seawater temperatures. Rapid deposition (>20 cm/ky; (Su et al., 2000)) of low-permeability turbiditic sediments and hemi-pelagic clay acts to hydrologically and thermally seal the underlying basaltic basement from seawater within a million years of crustal formation on the eastern flank of the JdFR. Consequently, the uppermost basement is conductively reheated as the underlying young oceanic lithosphere cools (Fisher, 2003).

The anomalously rapid sedimentation on top of young, hot, ocean crust on the JdFR's eastern flank produces strong lateral thermal, chemical and alteration gradients within the basement. Consequently the eastern flank of the JdFR has been the locus for extensive ridge flank geophysical, heat flow and hydrothermal explorations including three scientific ocean drilling expeditions (Davis et al., 1992, 1997; Fisher et al., 2005, 2011). Thirteen sites have been drilled along an 80 km age-transect perpendicular to the ridge axis on its eastern flank, in ocean crust ranging from 0.86 to 3.6 million years old (Davis et al., 1997). The variable sediment thickness (40–600 m) along the transect reflects the basement age and topography, which is dominated by ridge parallel normal-faulted ridges and valleys, and buried volcanic seamounts. Conductive heat flow and basement temperatures increase systematically with

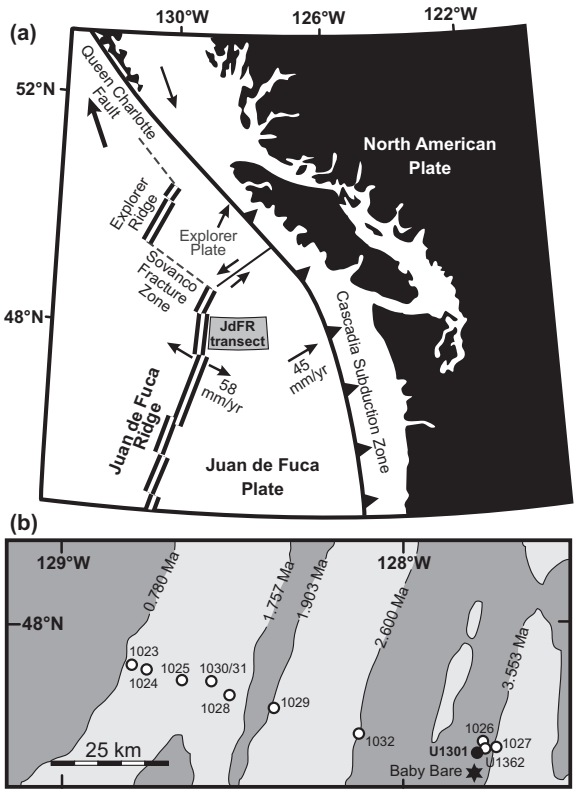

Fig. 1. Juan de Fuca Ridge location map and drill transect. (a) Regional map of the Juan de Fuca Plate showing the location of the JdFR drill transect (after Davis et al., 1997). (b) Magnetic anomaly map (dark gray shaded areas = positive anomaly, light gray shaded areas = negative anomaly) showing the ages of magnetic polarity transitions (Ma) and the locations of the JdFR transect drill sites (1023–1032; U1301 and U1362) and the Baby Bare vent site (after Davis et al., 1997; Underwood et al., 2005).

distance from the point of sediment onlap (Fisher et al., 2000). Sampled basement fluids reveal a progressive deviation from seawater chemistry with crustal age (Elderfield et al., 1999; Wheat et al., 2002, 2004) that is accompanied by an increase in the extent of basement alteration (Hunter et al., 1999; Marescotti et al., 2000). Cold seawater enters the permeable basement where it is exposed at the seafloor, circulates through the crust, and interacts with the basement rocks as it is heated (Fisher et al., 2000). Basement seamounts that penetrate through the overlying sediments provide permeable edifices through which seawater can enter or exit the crust or ridge flank, influencing basement fluid circulation patterns and reflecting a component of ridge-parallel fluid flow (Wheat et al., 2000; Fisher et al., 2003). For example, along Second Ridge, a basement ridge that runs sub-parallel to the spreading ridge ~100 km from its axis, thermal and chemical data reveal that seawater enters the crust through Grizzly Bare seamount (Becker and Fisher, 2000; Wheat et al., 2013) and flows ~50 km northeast along the ridge towards Baby Bare seamount (Fig. 1), where fluids vent at ~65 °C (Wheat and Mottl, 2000; Wheat et al., 2000; Fisher et al., 2003). The reaction of the fluid with the basement as it is heated leads to increases in fluid Ca^{+} and decreases in alkalinity, Mg^{2+}, Na^{+}, K^{+}, and $\delta^{18}O$ (Elderfield et al., 1999; Wheat and Mottl, 2000; Wheat et al., 2004, 2011). The basement fluids have low sulfate contents relative to seawater, that are thought to result from sulfate diffusion from the basement fluids into the overlying sediments (Elderfield et al., 1999). Ribosomal RNA gene sequencing of upwelling fluids sampled from ODP Hole 1026B (~1 km from Hole U1301B) indicate the presence of diverse bacteria and archea including sulfate reducing microbes (Cowen et al., 2003), although these may have originated from the sediment rather than the basement (Wheat et al., 2004). Sr-isotope exchange between seawater and basalt (with $^{87}Sr/^{86}Sr$ ratios of ~0.7092 and ~0.7025, respectively) results in an end-member ridge flank fluid Sr-isotopic composition of ~0.707 (Elderfield et al., 1999; Butterfield et al., 2001). Baby Bare spring fluids contain ~45 pmol/kg Tl, approximately 70% of the Tl concentration of seawater (Nielsen et al., 2006b), consistent with Tl-removal into upper crustal basalt on the ridge flanks.

3.2. Hole U1301B

IODP Hole U1301B was drilled at the eastern end of the JdFR transect in 3.5 Ma crust on Second Ridge approximately 6 km north-northeast of Baby Bare (Fisher et al., 2005). The circulation of seawater-derived ridge flank hydrothermal fluids through the basalt is sufficiently vigorous that the upper ~300 m of basement at Site 1301 is isothermal, at 64 °C (Fisher et al., 2005). Hole U1301B penetrates through the 265 m sedimentary section, which comprises turbidites overlying hemipelagic clay, and 318 m into the underlying basaltic basement. Given the brecciated and rubbly nature of the uppermost basement, the upper 86 m were cased but not cored. The cored basement interval (351–583 meters below seafloor, mbsf) consists of pillow lavas with minor massive basalt flows (up to 4.5 m thick) and rare hyaloclastite breccia intervals (<1 m thick). The basaltic rocks from Hole U1301B have N-MORB compositions. The lavas are sparsely to highly plagioclase ± olivine ± clinopyroxene-phyric and sparsely vesicular (1–5 vol% vesicles).

3.3. Hydrothermal alteration of U1301B basalts

Basalts from Hole U1301B exhibit slight to moderate alteration due to hydrothermal fluid–rock interaction that resulted in secondary mineral formation (Fisher et al., 2005). The secondary minerals replace the interstitial groundmass, line or fill vesicles and pore spaces, form veins (with the development of associated alteration halos), replace phenocrysts, and form the cements of the hyaloclastite breccias. The principal secondary minerals are saponite (a Mg-rich Fe^{2+} smectite), iron-oxyhydroxides, and celadonite (an Fe^{3+} mica), with minor sulfides and calcium carbonate. The basaltic lavas display dark gray 'background' alteration, due to groundmass replacement, vesicle-lining or filling and complete replacement of olivine phenocrysts by Mg-saponite. They are cut by 10 μm to 6 mm-wide hydrothermal veins, the majority of which are flanked by oxidative alteration halos; distinctly orange-brown colored

zones of the host rock typically 3–12 mm (up to 30 mm) wide. The halos exhibit a similar pattern of alteration (groundmass and phenocryst replacement and vesicle-fill) to the adjacent dark gray background altered basalts but contain celadonite ± Fe-oxyhydroxide in addition to Mg-saponite. The sulfide mineralogy of the background and halo samples is similar, but sulfide is less common in the halos. Many of the secondary sulfides appear to be recrystallized igneous grains. Sulfides occur as 1–10 μm interstitial, irregular grains of pyrite (the most abundant sulfide mineral), pyrrhotite, chalcopyrite, or pyrrhotite and chalcopyrite together. Plagioclase phenocrysts contain 1–2 μm inclusions of pyrrhotite, chalcopyrite, pyrite or chalcopyrite and either pyrrhotite or pyrite. In some instances a pyrite front of disseminated 120–350 μm secondary pyrite ± marcasite grains that fill pores and replace igneous silicates, 1–80 μm aggregates of pyrite + marcasite (pyrite replaces marcasite), and rare inclusions of chalcopyrite, separates the alteration halo from the dark gray background altered host rock. This suggests that there is a relationship between Fe oxidation and secondary pyrite formation (Ono et al., 2012).

4. ANALYTICAL METHODS

Fourteen samples from Hole U1301B were selected for analysis. Thin sections of the samples were examined using transmitted and reflected light microscopy, and the secondary mineral abundances were determined visually (Table 1). Phyllosilicate identification was based on optical properties in thin section. Saponite and celadonite are commonly intergrown to varying degrees, but based on experience with XRD and electron probe analyses, the presence of celadonite (or nontronite) with or without intergrown saponite can be distinguished from saponite alone based on optical properties (Alt, 2004). The presence of Fe-oxyhydroxides is readily apparent by red or brown coloring of phyllosilicates (Alt, 2004).

4.1. Sample preparation

Whole rock samples, including nine paired halo and background samples and two pyrite fronts, were cut using a diamond saw, crushed with a steel mortar and powdered in a tungsten carbide mill at the University of Michigan. Between 0.2 and 1.1 g of whole rock powder was dissolved in a 2:1 mixture of concentrated HF and HNO_3 for 24 h at 150 °C, evaporated until dry, re-dissolved in 6 M HCl, refluxed for 24 h, evaporated until incipient dryness, and re-dissolved in 6 M HCl. Aliquots of 5% from these solutions were taken for major and trace element analysis. The remainder of each sample solution was evaporated until near dryness and dissolved in 5 mL of 6 M HCl with 2% Br_2, to ensure total conversion of Tl^+ to Tl^{3+}.

4.2. Major and trace element analysis

The concentrations of selected major and trace elements were analyzed at the University of Southampton, where aliquots of the digested samples were dried down and dissolved in 2% HNO_3 containing 10 ng/mL In and Re, to give dilution factors of ~40,000 and 3000 for major and trace element analysis, respectively. The samples were analyzed on a Thermo X Series ICP-MS (Table 1 and Electronic Annex Table EA1), calibrated using international rock standards, with reference materials JA-2 and BHVO-2 run as unknowns. Uncertainties were better than 5% (1 RSD). The results are presented in Table 1 and Electronic Annex Table EA1.

4.3. Tl concentration and isotopic composition measurements

The Tl concentration and isotopic measurements were made at the MAGIC Laboratories of Imperial College London. The prepared solutions were processed using two stages of anion-exchange chromatography to separate Tl from the sample matrix, following previously developed techniques (Baker et al., 2009) modified to exclude the collection of Cd. Total procedural blanks contained <10 pg Tl. Tl isotope compositions were measured with a Nu Plasma multiple collector inductively coupled plasma-mass spectrometer (MC-ICP-MS), using previously described techniques that employ both external normalization to NIST SRM 981 Pb and standard-sample bracketing for mass bias correction (Baker et al., 2009). The anion exchange chromatography has been demonstrated to give quantitative Tl yields (Prytulak et al., 2013). The Tl concentrations of the samples were determined from their ^{205}Tl signal intensities during isotopic analysis, using internal standardization to the ^{208}Pb ion beam from the added SRM 981 Pb (Nielsen et al., 2006b; Prytulak et al., 2013). To monitor the accuracy and reproducibility of the Tl concentration and isotopic analyses, a basaltic reference material (BHVO-2) was analyzed multiple times. Ten separate dissolutions of BHVO-2 yielded an average Tl concentration of 18.2 ± 2.0 ng/g (1 sd) and $\varepsilon^{205}Tl = -1.5 \pm 0.3$ (2 sd), respectively. These values are in accord with published analyses of BHVO-2 (Table 2). Our BHVO-2 analyses combined with duplicate measurements of six of U1301B samples (Table 1) indicate that the uncertainties for our Tl concentration and isotopic measurements are ±10% (1 RSD) and ±0.3 ε-units (2 sd), respectively. Undissolved fluoride residues that result from incomplete HF–HNO_3 sample digestion have been shown to incorporate Tl from the sample solution and can hence compromise the Tl concentration measurements, although they do not fractionate the Tl isotopic composition of the solutions (Nielsen et al., 2005). Given the small sample sizes used here (0.2–1.1 g) and that repeated digestions of similar amounts of BHVO-2 consistently gave Tl concentrations within 10–20% of the published values, we are confident that any minor fluoride residues following HF-HNO_3 digestions did not significantly affect the Tl concentrations.

4.4. Sulfur concentrations

The sulfur contents of U1301B basalts were determined at the University of Michigan. Sulfur was extracted from the powdered whole rock samples by sequential acid extraction under N_2 atmosphere, with the evolved H_2S gas from

Table 1
Geochemistry and secondary mineralogy of U1301B altered MORB samples.

Sample:				Thallium:			Trace elements:		Sulfur[c]:				Mineralogy[d]:			Sulfides[e]:							
Sample	Lava[a]	Depth msb	Type[b]	Tl ng/g	ε^{205}Tl	±	Rb µg/g	Cs µg/g	AVS µg/g	CRS µg/g	Thode µg/g	ΣS µg/g	feox vol%	cel vol%	sap vol%	Abundance	py	po	cp	pn	mc	size µm	Pyrite front
U1301B:																							
4R2 45	P	103.2	BKG	18.2	−6.6	0.3	0.32	0.005	0	117	73	189	0	0	3	r	×					1–2	
			HALO	49.6	−2.3	0.3	7.50	0.239	0	272	11	283	3	15	3	r	×					1–2	120 µm (py)
			HALO-rpt	49.5	−1.9	0.3																	
4R2 122	P	104.0	BKG	20.6	−3.9	2.5	0.27	0.002	1	45	135	181	0	0	5	r	×					1–6	~300 µm (py + cp)
			HALO	80.5	−2.3	0.3	7.40	0.241	0	61	106	167	3	7	1	r	×		×			1–2	~300 µm (py + cp)
6R1 72	P	121.4	BKG	10.0			0.48	0.007	0	0	103	103	0	0	3	r		×				1–2	
			HALO	8.3	−3.1	0.3	5.80	0.275	0	12	45	57	4	7	1	r		×				1–2	
10R1 65	P	150.2	BKG	203	−10.5	0.3	0.34	0.005	0	384	1	385	0	0	3	r	×		×			1–4	
			BKG-rpt	202	−10.2	0.3																	
14R1 65	M	169.4	BKG	12.1			0.06	0.000	0	143	128	271	n.d	n.d	n.d	r	×	×	×			2–4	
			HALO	240	−8.1	0.3	4.93	0.104	0	339	116	455	n.d	n.d	n.d	c	×	×				4–10	some?
			PY FT	1494	−8.3	0.3	1.53	0.018	449	3788	139	4376	n.d	n.d	n.d	a	×				×	<100	300 µm (py + mc)
			PY FT-rpt	1494	−7.8	0.3																	
15R4 142	M	184.2	HALO	59.3	−10.1	0.3	10.94	0.317	0	41	32	73	n.d	n.d	n.d	m/c	×	×	×			1–10	
			HALO-rpt	59.4	−10.0	0.3																	
18R2 71	M	207.7	BKG	6.0	−3.4	0.3	0.91	0.009					0	0	10	a	×	×	×	×		2–50	
23R1 66	P	235.3	BKG	73.5	−7.0	0.3	0.61	0.016	0	253	115	368	n.d	n.d	n.d	r	×		×			1–4	1–10 µm (py)
			BKG-rpt	73.5	−6.8	0.3																	
			HALO	43.6	−4.3	0.3	11.29	0.432	0	82	27	109	3	7	1	r	×	×				1–5	1–10 µm (py)
24R1 117	P	241.8	BKG	5.0	−3.7	0.6	0.28	0.005	19	867	118	1004	0	0	12	a	×	×	×			2–20	
25R1 123	P	245.5	BKG	103	−7.1	0.3	0.17	0.001	35	94	212	341	0	0	2	r	×					1–5	
			HALO	26.0	−3.2	0.3	9.49	0.413	18	59	46	123	5	7	0	r	×					1–5	
			PY FT	32.8	−4.5	0.3	7.25	0.290	41	215	94	350	0	3	2	m	×				×	1–20	1–20 µm
30R1 119	P	271.1	HALO	7.4	−3.5	0.6	9.41	0.388	0	12	16	28	7	5	3	r							
32R3 50	P	288.2	BKG	184	−8.9	0.3	0.44	0.009	268	325	187	780	0	0	5	r	×					2–8	
			HALO	14.8	−7.2	2.5	11.24	0.377	1	69	57	128	7	7	1	r	×					2–8	

34R2 82	P	297.6	BKG		0.7	−1.0	1.0	0.84	0.013	0	tr	39		39	0	0	7	r		×		1–3
			HALO		1.2	−2.8	0.6	10.87	0.273	0	1	11		12	2	10	3	r	×			1–3
36R1 53	P	308.5	BKG		262	−4.7	0.3	0.89	0.018	72	178	97		347	0	0	2	m		×		1–3
			HALO		16.2	−4.6	0.4	10.31	0.346	0	76	35		112	3	7	3	r		×		1–3

n.d = not determined; tr = trace.
[a] P = pillow flow; M = massive flow.
[b] BKG = background; PY FT = pyrtite front; rpt = sample repeat.
[c] AVS = acid-volatile sulfide; CRS = chromium-reduced sulfide; ΣS = AVS + CRS + Thode.
[d] feox = Fe-oxyhydroxide; cel = celadonite; sap = saponite.
[e] r = rare; m = moderate; c = common; a = abundant; py = pyrite; po = pyrrhotite; cp = chalcopyrite; pn = pentlandite; mc = marcasite; × = present.

each sulfur fraction precipitated as Ag_2S (Rice et al., 1993). The acid-volatile sulfide (AVS, monosulfide) fraction was extracted by reaction in 6 M HCl with $SnCl_2$. The chromium-reduced sulfide (CRS, or pyrite) fraction was extracted using an acidified $CrCl_2$ solution. Residues were then reacted with Thode's solution ($HCl + H_3PO_2 + HI$; (Thode et al., 1961)) to reduce sulfate to H_2S. The whole rock sulfur contents for each fraction were determined gravimetrically using Ag_2S precipitates. Sulfur extractions from mixtures of international reference materials (NBS 123 sphalerite, NBS 127 barite and Park City Pyrite) were within 5% of the expected values for each S phase, and total S was within 3% of the expected value (Electronic Annex Table EA2).

5. RESULTS

Samples that display background alteration contain between 2 and 12 vol% Mg-saponite (Table 1 and Fig. 2). The halos typically contain less Mg-saponite than the adjacent background altered basalt (0–3 vol%) but the addition of celadonite and Fe-oxyhydroxide results in a greater total volume of secondary minerals in the halos (11–21 vol%). Sulfide minerals were observed in all samples, with no obvious distinction in their abundance between background and halo portions (Table 1).

The samples contain between approximately 1 and 1500 ng/g Tl and have ε^{205}Tl values in the range of approximately −1.0 to −10.5 (Table 1). The samples that are most enriched in Tl with respect to fresh MORB generally have the most fractionated isotopic compositions (Fig. 3). However, there is significant variability in the Tl isotopic composition at a given Tl content. The relationship between Tl concentration and Tl isotopic compositions of U1301B samples is consistent with previous observations from ODP Hole 504B (Nielsen et al., 2006b). However, the U1301B basalts do not show the systematic decrease in the extent of Tl-enrichment and Tl isotopic fractionation with depth that samples from Hole 504B revealed (Fig. 4). Rather, U1301B samples display a range of Tl concentrations and ε^{205}Tl at a given depth, with two samples from near the bottom of Hole U1301B (~300 msb) significantly enriched in Tl relative to fresh MORB (Fig. 4). The U1301B analyses include seven pairs of background and halo samples for which both Tl concentration and ε^{205}Tl were determined. Neither the halo nor background portion consistently has the greatest Tl content. However, for six of the pairs the background portions contain Tl that is isotopically lighter than the corresponding halo. The only exception is a pair for which both the halo and background portion have Tl concentrations and isotopic compositions within the range of fresh MORB glass.

To investigate whether Tl-uptake during low temperature hydrothermal alteration of ocean floor basalts is associated with a particular secondary mineral, we plot the Tl content of the samples versus their estimated Mg-saponite, celadonite, and Fe-oxyhydroxide contents (Fig. 5). However, there is no observed association between Tl content and the modal proportions of these secondary minerals.

Table 2
Thallium analyses of BHVO-2.

References	Tl (ng/g)	±1 sd	ε^{205}Tl	±2 sd	*n*	*d*
Baker et al. (2009)	–	–	−2.1	0.5	2	2
Prytulak et al. (2013)	17.9	1.0	−1.5	0.4	2	2
This study	18.2	2.0	−1.5	0.3	11	10

n = number of runs, *d* = number of dissolutions.

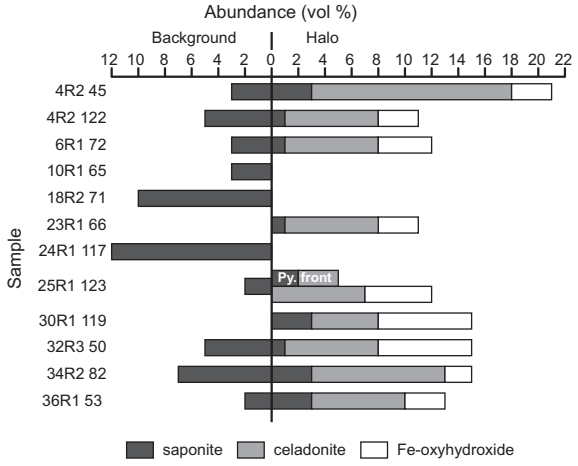

Fig. 2. U1301B sample secondary mineralogy. The proportions of secondary minerals (Mg-saponite, celadonite and Fe-oxyhydroxide) in the background, halo and pyrite front (Py. Front) portions of the samples analyzed in this study.

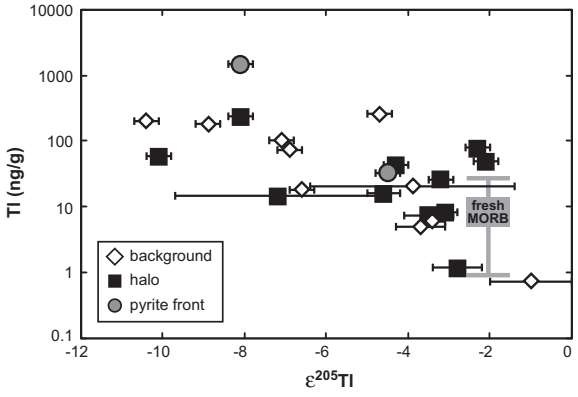

Fig. 3. Thallium concentration versus thallium isotopic composition of Hole U1301B samples. Open diamonds = background samples, black squares = alteration halos, and gray circles = pyrite front samples. The range in composition of fresh MORB glass (Nielsen et al., 2006b) is shown for comparison (gray box).

The Hole U1301B basalts analyses reveal excellent correlations between Rb and K ($R^2 = 0.93$, $n = 14$; Fig. 6a) and Rb and Cs ($R^2 = 0.93$, $n = 24$; Fig. 6b), whereby the alkali elements are enriched in the halos compared to the background samples. Paired analyses of the background and halo portions of a given sample allow the extent of enrichment of a trace element in the halo relative to the

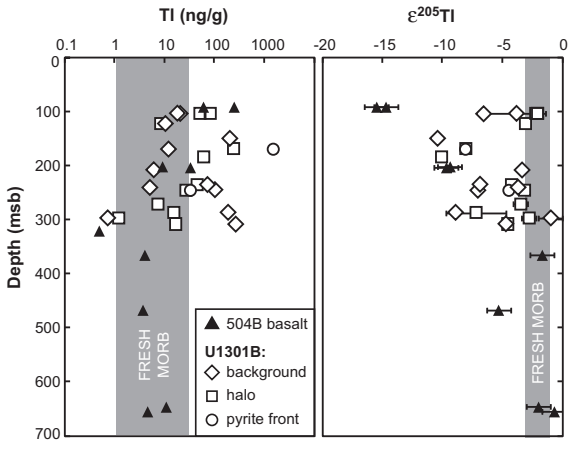

Fig. 4. Variations in Tl concentration and Tl-isotopic composition with depth in Holes U1301B and 504B. Black triangles = 504B whole rock samples (Nielsen et al., 2006b); U1301B samples: symbols as in Fig. 3. The range in Tl concentration and isotopic composition of fresh MORB glass (Nielsen et al., 2006b) are shown for comparison (gray bar).

adjacent background to be quantified, using a trace element enrichment factor (EF):

$$EF_X = \frac{X_{HALO}}{X_{BKG}} \quad (2)$$

where X_{HALO} and X_{BKG} are the concentrations of trace element X in the halo and background portions of the sample. The celadonite and Fe-oxyhydroxide bearing halos are significantly enriched in both Rb and Cs relative to the saponitic background altered samples, with enrichment factors in the range 12–90 and 19–413, respectively. The greater extent of Cs uptake compared to Rb is consistent with previous analyses of ocean crustal basalts (Hart, 1969). The higher Rb and Cs concentrations of the celadonite-bearing halos compared to the saponitic background reflect the substitution of Rb^+ and Cs^+ for K^+ in celadonite. In contrast, the ranges in Tl content for the background and halo samples are indistinct, and there is no relationship between Tl and Cs, Rb, or K (Fig. 6).

Correlations were sought between Tl concentrations and all other analyzed trace elements (Electronic Annex Table EA1). Thallium was found to correlate significantly only with the sulfide (AVS + CRS) sulfur content ($R^2 = 0.92$, $n = 22$; Fig. 6f). The enrichment factors for S (AVS + CRS; 0.1–2.4) and Tl (0.1–20) are highly variable, with Tl and S concentrations higher in the background than in the halo of some samples, but lower in the background

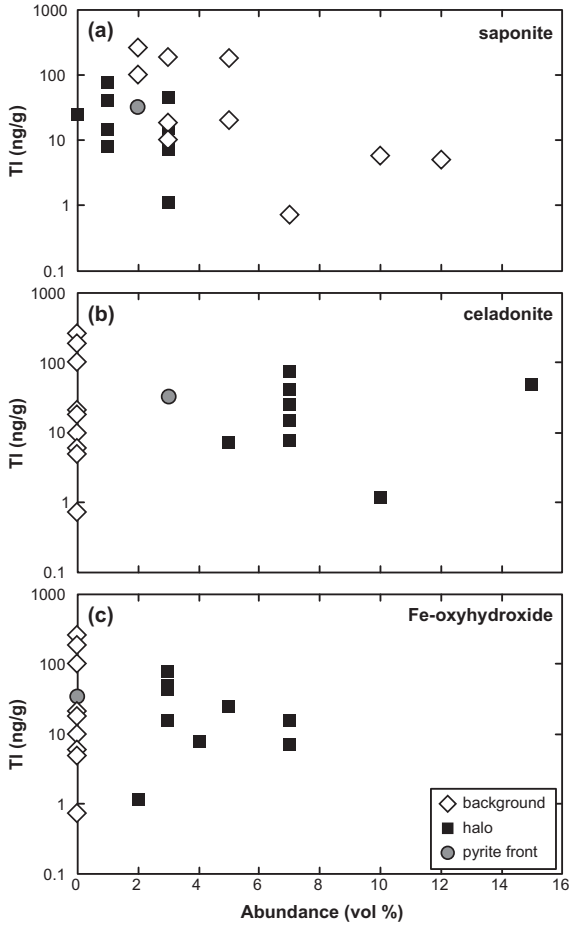

Fig. 5. Tl concentration versus secondary mineral abundance in IODP Hole U1301B altered basalts. (a) Mg-saponite; (b) celadonite; and (c) Fe-oxyhydroxide. Symbols as in Fig. 3.

than in the halo for others. There is no relationship between Tl and the sulfate component of the S content and Tl does not correlate with any of the analyzed chalcophile elements (Pb, Sn or Cu).

6. DISCUSSION

6.1. Tl-uptake by MORB exposed at the seafloor

In the following, we first discuss the Tl-uptake that is associated with alteration of MORB at the seafloor, to highlight how these processes differ from the reactions that affect Tl during hydrothermal alteration within conductively reheated sections of upper ocean crust. We therefore consider the chemistry of MORB samples that were dredged from the seafloor where they were exposed to large volumes of cold seawater, although they may also have been previously altered by low temperature hydrothermal fluids. During seafloor alteration, the alkali elements K, Rb and Cs are enriched in MORB, with Rb^+ and Cs^+ preferentially incorporated into the K^+-bearing silicate minerals such as K-feldspar and celadonite (Hart, 1969). Previous studies of Tl-uptake by MORB provide some evidence that Tl may behave in a similar manner to the alkali elements during alteration of MORB at the seafloor (McGoldrick et al., 1979). Here we use published K, Rb, Cs and Tl concentrations of dredged MORB to re-investigate this assertion.

The database encompasses samples from the fast spreading East Pacific Rise (EPR) (Jochum and Verma, 1996) and the slow-spreading Mid Atlantic Ridge (McGoldrick et al., 1979), and includes paired samples of variably altered portions of the same protolith (e.g., the altered core of a pillow lava and its fresher glassy rim). The data reveal a positive correlation between the K and Rb abundances, which falls within the array of fresh MORB compositions. The more altered portions of paired samples have higher K and Rb concentrations than their fresher counterparts (Fig. 7a) consistent with the enrichment of alkali elements in MORB through interaction with seawater. All altered dredge samples are also enriched in Tl relative to fresh MORB glass (Fig. 7b) but there is no clear correlation between Tl and K concentrations. There is, however, a weak correlation between Tl and Rb ($R^2 = 0.37$, $n = 15$), and the more altered portion of a paired sample typically has higher Cs, Rb and Tl concentrations than the fresher counterpart (Fig. 7). Based on this, we conclude that the compiled results indicate that seafloor alteration of MORB is associated with Tl and alkali uptake from seawater. However, given the lack of a clear relationship between Tl and K in dredged MORB (Fig. 7a), the uptake of Tl and the alkalis during seafloor weathering does not appear to be fully coupled, for example by incorporation into the same mineral, but may involve, at least in part, different processes and/or phases.

6.2. Controls on Tl-uptake and Tl-isotope fractionation at Site U1301

The mineralogical and geochemical analyses of Hole U1301B basalts are consistent with Tl-uptake occurring as a result of its incorporation into secondary sulfides rather than secondary silicate minerals. The highly variable enrichment factors for S and Tl are consistent with the presence of secondary sulfide minerals in both background and halo sample portions, and may in part result from the occurrence of microscopic pyrite fronts that are not visible in hand specimen and may therefore have been variably included in either the halo or background portion (or both) of a sample during mechanical separation of the two alteration zones. The lack of correlation between Tl and the chalcophile elements Cu, Pb and Sn is probably a consequence of the extremely low primary magmatic Tl concentration. Hence, the Tl added during hydrothermal alteration completely dominates the present Tl budget of the rocks. In contrast, the other chalcophile elements have higher concentrations in fresh MORB and consequently their budget is divided between primary phases and the hydrothermal contributions of secondary sulfides.

The isotopic analyses of the paired background-halo samples indicate that the Tl added to the background is more fractionated (with more negative ε^{205}Tl) than that added to the adjacent halos, irrespective of which portion contains the most Tl (Table 1 and Fig. 4). This could

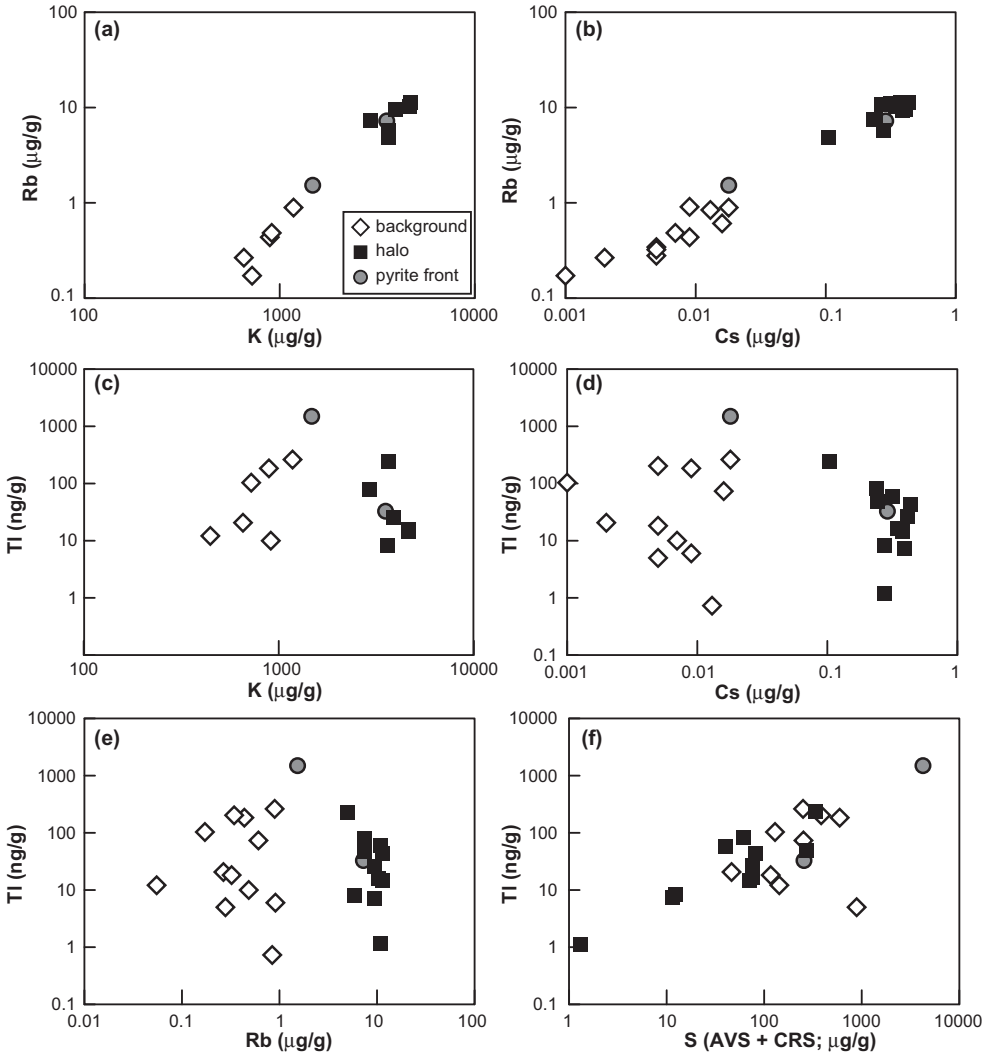

Fig. 6. Comparison of trace element concentrations in IODP Hole U1301B altered basalts. (a) Rb vs K; (b) Rb vs Cs; (c) Tl vs K; (d) Tl vs Cs; (e) Tl vs Rb; and (f) Tl vs S (sulfide sulfur). Symbols as in Fig. 3.

reflect mineralogical, physical, or chemical control on Tl-uptake, or may be an artifact of insufficient sampling. Pyrite (FeS_2; cubic) and pyrrhotite ($Fe_{(1-x)}S$; $x = 0$–0.17) occur in both background and halo samples, whereas chalcopyrite ($CuFeS_2$) was observed in six background samples but was rare in the halos, and marcasite (FeS_2; orthorhombic) was only documented in pyrite fronts (Table 1). As Tl is correlated with both acid volatile (e.g., pyrrhotite) and chrome reducible (e.g., pyrite) sulfide and there are no samples that contain only the former, our data cannot constrain whether Tl-uptake is associated with one or more sulfide phases.

The mass balance inferred from the elemental systematics (Fig. 6) indicates the observed Tl-isotope fractionation signatures are also primarily governed by sulfides rather than secondary silicate phases. If Tl is incorporated into more than one sulfide mineral, the different isotope fractionation factors of these phases could account for the lighter isotopic compositions of Tl in the background samples relative to the adjacent halos. Alternatively, if Tl is only present in a single sulfide phase, the fractionation of isotopically light Tl into the background relative to the halo may reflect the different physical/chemical conditions on either side of the halo-background boundary, which is interpreted to be a redox front (Ono et al., 2012).

6.3. Tl-uptake within ocean crust: comparison with Holes 504B and 896A

To evaluate the processes that affect Tl-uptake within the ocean crust, we compare our analyses of JdFR basalts to those of basaltic lavas from ODP Holes 504B and 896A on the southern flank of the Costa Rica Rift in the Eastern Equatorial Pacific. Hole 896A lies 1 km to the southeast of 504B, on a local basement high, and penetrates through the 179 m thick sediment and 290 m into the underlying volcanic basalts (Teagle et al., 1996). The paired holes allow investigation of the effects of basement hydrology on hydrothermal alteration, since Hole 896A is located in a ridge flank hydrothermal upflow zone whereas 504B is

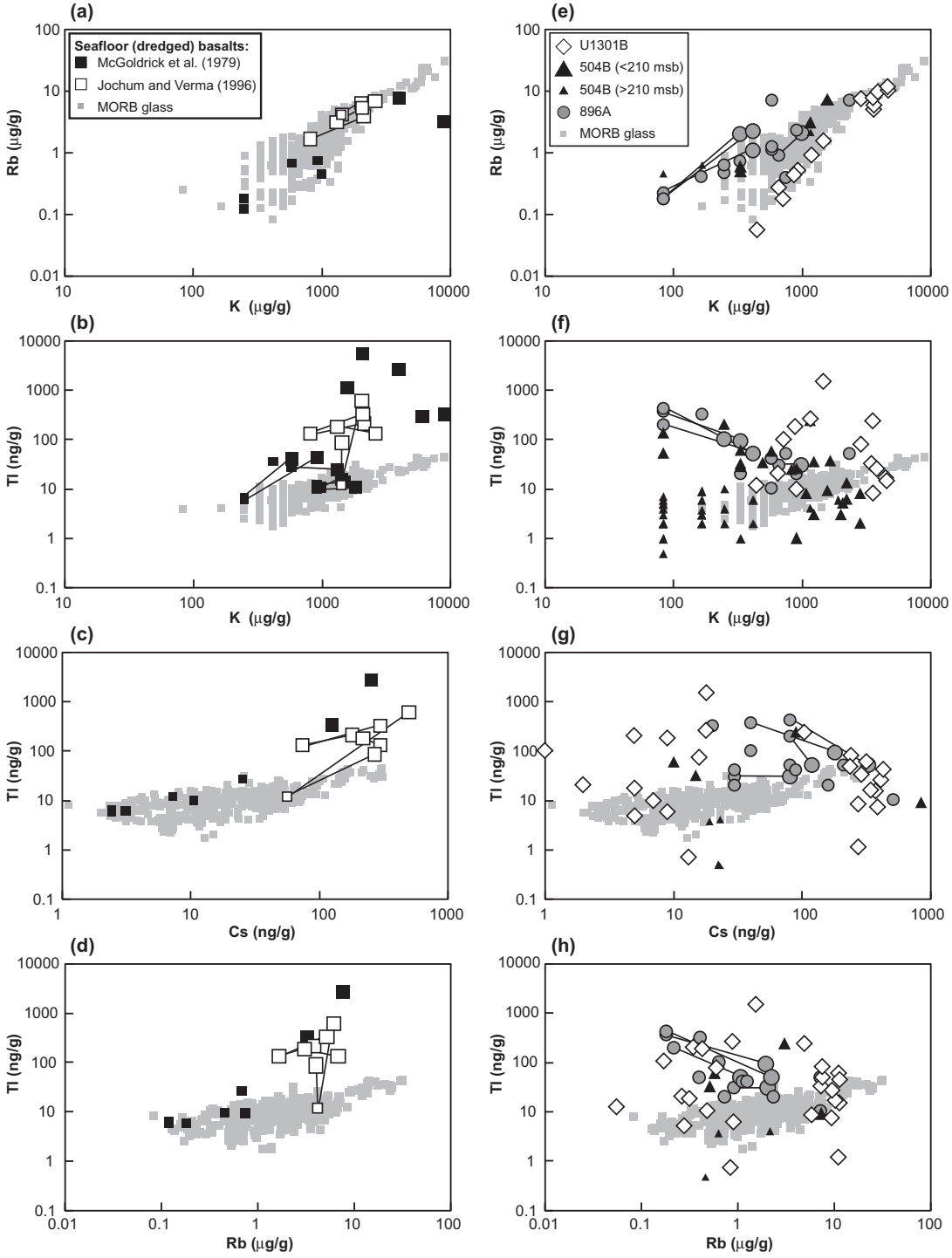

Fig. 7. Trace element concentrations of dredged seafloor basalt samples (a–d) and basalts from Holes 504B, 896A, and U1301B (e–h). (a and e): Rb vs K; (b and f): Tl vs K; (c and g): Tl vs Cs, and (d and h): Tl vs Rb. (a–d): black squares = samples dredged from the MAR (McGoldrick et al., 1979), white squares = samples dredged from the EPR (Jochum and Verma, 1996); variably altered paired samples from the same protolith are joined by tie lines, with the small squares indicating the fresher portion of the sample and the large square indicating the more altered portion. (e–h): open diamonds = Hole U1301B, black triangles = Hole 504B (large triangles = samples from above 210 msb) (Hubberten et al., 1983; Alt et al., 1996b; Nielsen et al., 2006b), gray circles = Hole 896A (Teagle et al., 1996). Tie lines join paired 896A red halo (larger circles) and background samples from the same protolith. The compositions of fresh MORB glasses are shown for comparison (light gray squares; (Jenner and O'Neill, 2012)).

in an area of ambient heat flow (Alt et al., 1996a). The volcanic stratigraphy, physical properties, geochemistry and hydrothermal alteration of Hole 504B and 896A volcanic rocks have been described in detail elsewhere (e.g., Alt et al., 1986, 1996a; Teagle et al., 1996; Bach et al., 2003 and references therein) and are briefly summarized here.

6.3.1. Holes 504B and 896A

The alteration of Hole 504B lavas reflects the evolution of the system from open circulation of cold (<40 °C) oxidizing seawater to more restricted circulation of less-oxidative, evolved seawater-derived fluids (at <140 °C), as the crust is isolated from the ocean by sediment and fractures in the basalts are sealed by vein-filling minerals (Alt et al., 1996b). The volcanic section of Hole 504B is divided into two alteration zones, on the basis of macroscopic alteration features and geochemical analyses (Alt et al., 1996b). Dark gray 'saponitic' background altered basalts occur throughout. The more permeable upper 320 m of the volcanic section also contains reddish Fe-oxyhydroxide-bearing halos and celadonite-bearing black halos, which flank fractures and veins. Such oxidative alteration halos are absent in the lower volcanic zone (320–570 msb) where pyrite-bearing Mg-saponite veins occur. The upper zone has high concentrations of K, Rb, Mg, and H_2O and elevated $\delta^{18}O$, δD and $^{87}Sr/^{86}Sr$, as a result of open circulation of cold seawater during the first stage of alteration (Alt et al., 1996b; Bach et al., 2003). The greatest chemical changes occur in the oxidative alteration halos and breccias. Similar chemical changes are observed in the lower volcanic zone, albeit to a lesser extent. The subsequent formation of Mg-saponite and pyrite under higher temperature (<140 °C) and less-oxidizing conditions resulted in increased Mg, H_2O, and $\delta^{18}O$, a slight increase in alkalis and local gains of S throughout the lava sequence. The $Fe^{3+}/\Sigma Fe$ ratio is also elevated throughout the volcanic section relative to fresh glass (0.14–0.2), with slightly higher $Fe^{3+}/\Sigma Fe$ ratios in the visibly oxidized upper volcanics (0.40 ± 0.06) compared to the lower volcanics (0.33 ± 0.07) (Bach et al., 2003) (Fig. 8). Oxidation of the primary sulfides (pentlandite, pyrrhotite, and chalcopyrite) is responsible for pervasive S-depletion of the upper volcanic zone relative to fresh glass (~900 ppm Sulfur) (Alt et al., 1996b; Bach et al., 2003). In contrast, the formation of secondary pyrite in the lower volcanics resulted in S redistribution rather than net S loss (Fig. 8).

The lavas from Hole 896A are lithologically and geochemically similar to those from Hole 504B, with a slightly higher proportion of massive flows relative to pillow lavas in the former (Alt et al., 1996a). The alteration of the 896A lavas and the associated geochemical changes are similar to those observed in the upper 504B volcanics (Teagle et al., 1996). The lavas exhibit dark gray background saponitic alteration, with oxidized red halos flanked by well-developed pyrite fronts. Late stage $CaCO_3$ and thick Mg-saponite veins are more abundant at the upwelling site (896) (Alt et al., 1996a) and there is a slight decrease in the iron oxidation ratio ($Fe^{3+}/\Sigma Fe$) with depth in the Hole 896A volcanics (Fig. 8). Sulfur contents are variable with depth (Fig. 8), and primarily relate to the alteration styles. Saponitic gray rocks have S contents similar to, or enriched relative to, fresh glass, whereas Fe-oxyhydroxide and celadonite bearing halos are depleted in S (Teagle et al., 1996). These data are consistent with the observed replacement of primary sulfides by Fe-oxyhydroxide in the oxidative halos, and the development of secondary pyrite in the adjacent dark gray background saponitic basalts.

6.3.2. Comparison of Tl-uptake in Holes 504B, 896A and U1301B

Previous studies of the Tl content of 504B and 896A lavas report a correlation between the Tl and S contents of 896A lavas (Teagle et al., 1996), but suggest that Tl behaves differently in 504B where Tl is enriched in the oxidized upper volcanics that are on average alkali-enriched and S-depleted, but not in the sulfide-bearing lower

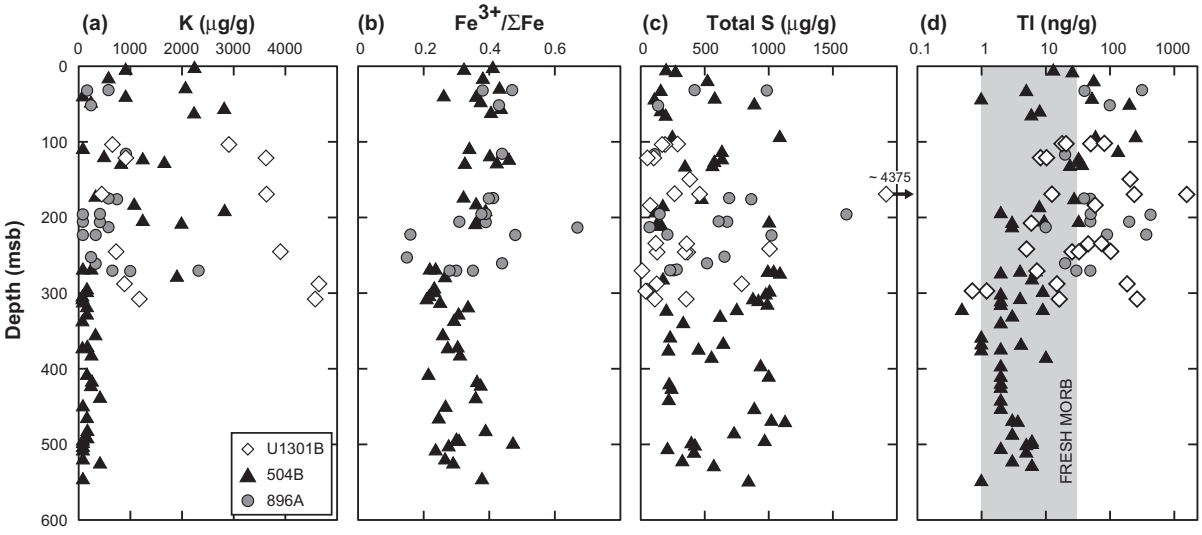

Fig. 8. Geochemistry of altered basalts from Holes 504B, 896A and U1301B, plotted versus depth in basement. (a) K (wt%); (b) $Fe^{3+}/\Sigma Fe$; (c) S; and (d) Tl. Open triangles = U1301B, black triangles = 504B (Hubberten et al., 1983), and gray circles = 896A (Teagle et al., 1996).

volcanics (Hubberten et al., 1983; Teagle et al., 1996) (Fig. 8). Here we re-evaluate these data, and compare them with the evidence from Hole U1301B.

The basalts from Holes 896A and U1301B typically have K, S and Tl contents within the range of volcanic rocks from the upper ~200 m of Hole 504B (Fig. 8), although Hole 896A lavas have higher S and lower K abundances at a given depth than the Hole 504B lavas. The K concentrations of U1301B basalts show a bi-modal distribution because the celadonite-bearing halos contain 3–4 times more K than the dark gray background altered samples. Notably, significant Tl-enrichments (>30 ng/g Tl) are observed throughout the ~300 m thick drilled sections of the Hole 896A and U1301B volcanics, but are limited to the upper ~200 m at Hole 504B (Fig. 8). Despite the observed enrichment of Tl in the K-enriched upper volcanics of Hole 504B, there is no positive trend between Tl and K, Cs or Rb in either Hole 504B or 896A (Fig. 7f–h).

The lack of correlation between Tl and the alkalis does not rule out the incorporation of Tl into an alkali-bearing mineral. However, paired background saponitic samples and red alteration halos from Hole 896A reveal that the halos are enriched in K, Rb and Cs relative to the background portions of the same samples whereas Tl is enriched in the background relative to the halo (Fig. 7e–h). Since the paired background and halo samples experienced the same thermal history and interacted with fluids that underwent the same geochemical evolution as it passed through the crust, the differences in Tl, Cs and Rb uptake by the halo and the adjacent background are most likely either a mineralogical effect or due to the different geochemical conditions that were prevalent on either side of the redox front along the margins of the halo. As fluid diffuses away from a fracture into the wall rock, the alteration phases precipitated depend on the extent of fluid–rock reaction and the oxidizing potential of the fluid, with Tl enrichment occurring in the host rock from fluid that evolved as it passed through the halo. The difference in the Tl content of the halo and background samples is likely more obvious in samples from Hole 896A than in Hole U1301B rocks because more distinctly defined halos allowed a better mechanical separation of the two portions in the former lavas. The published Hole 504B and 896A data are therefore in accord with our analyses of JdFR basalts and support the conclusion that Tl-uptake during hydrothermal circulation within the upper ocean crust is not primarily associated with the formation of alkali-bearing secondary silicate minerals.

Taken in its entirety, the Hole 504B dataset does not show a correlation between the Tl and S contents of the volcanic rocks. However, if we only consider the uppermost 210 m of the Hole 504B volcanic zone, the region in which Tl is clearly enriched relative to fresh MORB glasses, the Tl content does correlate with S ($R^2 = 0.68$, $n = 19$) as observed in Holes U1301B and 896A, despite a net loss of S from these rocks (Fig. 9). In contrast, the deeper volcanics that retained or gained S through secondary sulfide formation with no significant gain in Tl show no relationship between Tl and S. Assuming that Tl-uptake occurs as a result of Tl incorporation into secondary sulfide, rather than adsorption onto primary sulfide, the relationship between S and Tl despite a net depletion of S in the Hole 504B upper volcanics, indicates that the remaining sulfide was partially or completely recrystallized during hydrothermal alteration of this zone. This is consistent with observations from ODP Holes 801C and 1256D, where the rocks gained S through seawater sulfate reduction, resulting in seawater-derived sulfur in secondary sulfides, despite exhibiting a net loss of S as a result of oxidation (Rouxel et al., 2008; Alt and Shanks, 2011).

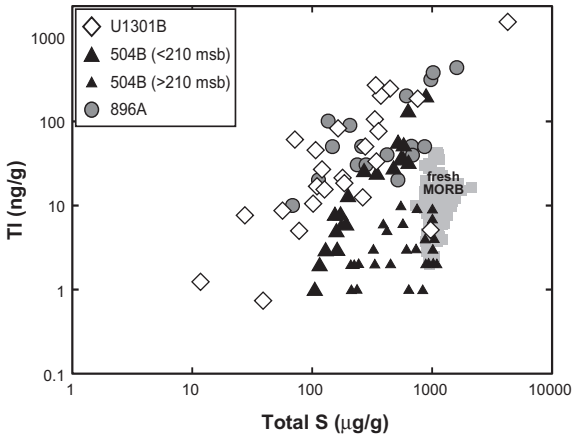

Fig. 9. Thallium concentrations of altered basalts from Holes 504B, 896A and U1301B versus S concentration. Open triangles = U1301B (sulfide-S only), black triangles = 504B (large triangles = samples from above 210 msb) (Hubberten et al., 1983), and gray circles = 896A (Teagle et al., 1996). The compositional range of fresh MORB glasses (Alt et al., 1996b; Bach et al., 2003; Nielsen et al., 2006b) are shown for comparison (gray box).

The most S-rich samples from Hole 896A are typically the saponitic rocks (Teagle et al., 1996), which also exhibit the greatest Tl-enrichments relative to fresh glass. This is in contrast to the majority of other elements (including K, Rb, Cs), for which the greatest changes in concentration occur in halos and breccias (Teagle et al., 1996; Alt et al., 1996b; Bach et al., 2003). The observed Tl-S trends for Holes 504B, 896A and 1301B are distinct (Fig. 9). The Hole 504B samples typically have lower Tl concentrations at a given S content than Hole 896A and U1301B rocks. Possible explanations include: (i) a difference in the extent of Tl partitioning into the secondary sulfide(s) due to differences in secondary sulfide mineralogy or local conditions (e.g., temperature, oxidation state); (ii) differing proportions of primary and secondary sulfide at each site, if Tl-uptake is only associated with the development of secondary sulfide; (iii) a greater proportion of sulfate sulfur that is not associated with Tl-uptake at Hole 504B; or (iv) a greater flux of fluid through Site 896 that enhanced Tl addition to the crust.

6.4. Controls on Tl-uptake: implications for hydrothermal fluid flux calculations

The evidence from Holes 504B, 896A and U1301B demonstrates that Tl-uptake during hydrothermal alteration of

the ocean crust is associated with the S-content of the basalts, indicating that Tl is most likely incorporated into secondary sulfides. Given this conclusion, it is perhaps counter-intuitive that significant Tl-enrichment in Hole 504B is restricted to the uppermost basalts through which there was circulation of oxidizing fluids, rather than the underlying lavas where conditions were more reducing and secondary sulfide more abundant. The distance to which advective transport displaces the signature of a geochemical tracer through the ocean crust is proportional to the time integrated fluid flux, but also depends on the relative concentration of the tracer in the fluid (C_{fluid}) and the rock matrix (C_{rock}) (Bickle and Teagle, 1992). The concentration of S in seawater and basalt are similar (~900 ppm), whereas for Tl, the system is rock dominated ($Tl_{fluid}/Tl_{rock} \sim 4 \times 10^{-3}$). Consequently, a much higher fluid flux is required to advect a Tl-isotopic signature to a given depth in the crust and a decoupling of S and Tl-uptake is therefore expected for the lower Hole 504B lavas.

Given that there is a clear depth limit to Tl-uptake in the Hole 504B crust, which coincides with a mineralogically and chemically defined alteration boundary, we pose the question: is Tl-uptake by the ocean crust limited by the Tl content of the hydrothermal fluid, or the conditions in the crust? This has significant implications for Tl-based calculations of hydrothermal fluid fluxes, and the extrapolation of the results to other crustal sites. If the depth of Tl-uptake is limited by the availability of Tl in fluids, which exhibit decreasing Tl content with increasing depth due to removal of the element from the fluid into the basalt, then a Rayleigh fractionation model (Nielsen et al., 2006b) is valid. However, if the alternative scenario applies, whereby Tl-uptake is limited by the physical or chemical conditions in the crust (e.g., temperature, oxidation state), then we need to understand which factors control Tl partitioning into sulfides to properly interpret the Tl budget of the ocean crust. Significant Tl-enrichments are observed to greater depths in Holes 896A and U1301B compared to Hole 504B, indicating that either differences in the hydrogeology resulted in deeper penetration of Tl-bearing fluids at those sites, or the conditions favored Tl-uptake at deeper levels in the crust. Unfortunately, since the depth limit to Tl-uptake has not been reached at either site, it is not possible to determine whether this coincides with a change in the physical or chemical conditions within the crust.

The hydrothermal system within the ocean crust varies not only with depth, but also with distance from the ridge axis (Alt et al., 1986). The system evolves with time as the crust moves away from the axial magmatic heat source and is sealed from the oceans by sediments, causing changes in the thermal, hydrological, and chemical conditions. The conditions also vary spatially within the crust, even over a few centimeters, as a function of distance from the fluid flow pathways and hence fluid/rock ratio (Alt, 2004; Alt and Teagle, 2003). The association between Tl and S indicates that Tl-uptake by the ocean crust depends on the fluid flux associated with alteration of the ocean crust that involves secondary sulfide-precipitation. A similar general sequence of alteration is recorded by upper volcanic rocks from Sites 504, 896 and 1301 (Teagle et al., 1996; Alt et al., 1996a; Fisher et al., 2005):

(1) Early (on-axis) development of celadonite-bearing dark halos from low temperature hydrothermal fluids.
(2) Fe-oxyhydroxide rich halos develop adjacent to fractures, as a result of circulation of oxidizing seawater, with the concurrent formation of Mg-saponite and pyrite under more reducing conditions in the adjacent host rock where fluid/rock ratios are lower. The pyrite may be concentrated along the redox boundary between the halo and the host rock, forming a pyrite front. The gradual advance of the redox boundary into the host rock can result in the superimposition of the Fe-oxyhydroxide rich halo upon earlier Mg-saponite.
(3) Precipitation of Mg-saponite + pyrite ± $CaCO_3$ in fractures and throughout the rock, as the conditions become more reducing, and the fluids are more evolved.
(4) $CaCO_3$ ± zeolite forms in fractures.

Although open circulation of seawater through the crust (stage 2) results in oxidation and net S-loss from the lavas, these effects are restricted to the halos and are accompanied by localized S-uptake in pyrite fronts and disseminated sulfides in the adjacent background rock (Fig. 10). Hence, paradoxically, a higher flux of oxidizing seawater should result in greater Tl-uptake even though Tl is hosted in sulfide minerals that form in reducing environments. Since Tl-uptake is also expected during stage 3, Tl is a useful tracer of fluid rock interaction for both 'open' and 'restricted' flow conditions. However, an understanding of the local thermal history and hydrogeology is necessary to constrain the timing and duration of these events at a particular site.

Our results indicate that Tl-uptake by the ocean crust requires both a sufficient flux of Tl-bearing fluids and the formation of secondary sulfides as a Tl-sink. Evidence from several sites, including Hole U1301B, ODP Hole 1256D in 15 Ma eastern Pacific crust, and ODP Hole 801C in the Jurassic crust of the western Pacific, suggests secondary sulfides can form as a result of microbial sulfate reduction (Rouxel et al., 2008; Alt and Shanks, 2011; Ono et al., 2012; Lever et al., 2013). Secondary sulfides from Holes 801C, 1256D and U1301B exhibit mass-dependent equilibrium S isotope fractionations relative to seawater sulfate, which are consistent with sulfate reduction at low temperatures (<70 °C) (Rouxel et al., 2008; Alt and Shanks, 2011; Ono et al., 2012). Functional genes indicative of sulfate-reducing microorganisms have been detected in basalts from Hole U1301B (Lever et al., 2013). Sulfur-based metabolic activity of the sub-surface biosphere therefore influences the global sulfur budget in the oceanic crust (Rouxel et al., 2008).

Sulfur isotope systematics ($\Delta^{33}S$–$\delta^{34}S$) provide constraints on whether sulfides in basalts are primary (mantle-derived), hydrothermal, or microbial in origin (Ono et al., 2012). The S isotope systematics for the majority of

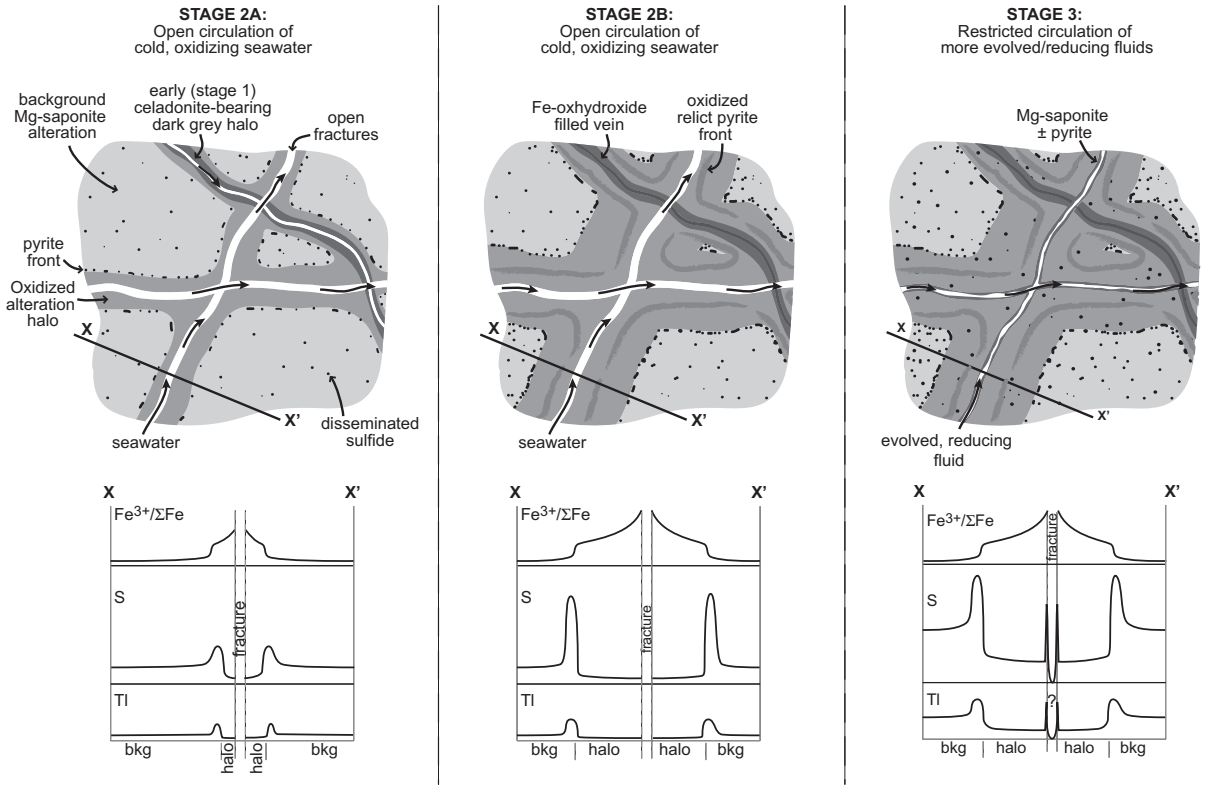

Fig. 10. Cartoon showing the progressive low-temperature alteration and associated relative changes in $Fe^{3+}/\Sigma Fe$, S and Tl concentrations of a piece of upper crustal basaltic lava. Celadonite-bearing dark halos form from low-temperature hydrothermal fluids on axis during stage 1 (not illustrated). As the crust moves off axis cold oxidizing seawater circulates through the crust (stage 2). Fe-oxyhydroxide-bearing halos develop adjacent to the fractures (stage 2A) with pyrite forming in a front along the redox boundary between the halo and the adjacent host rock, where Mg-saponite and disseminated pyrite form under more reducing conditions. Ongoing circulation of cold seawater (stage 2B) causes the redox boundary to migrate into the host rock, resulting in oxidation of the previously developed pyrite front. As fluid circulation becomes more restricted (stage 3) Mg-saponite + pyrite ± $CaCO_3$ precipitate in fractures and throughout the rock. Late stage $CaCO_3$ ± zeolites precipitate in fractures during stage 4 (not illustrated). The relative changes in $Fe^{3+}/\Sigma Fe$, S and T concentrations away from a fracture during stages 2A, 2B and 3 are indicated (not to scale). Tl-uptake is primarily associated with secondary sulfide formation in the migrating pyrite front during stages 2A and 2B, with more pervasive S and Tl-uptake during stage 3.

Hole 1301B basalts cannot be explained by equilibrium hydrothermal sulfate reduction, and indicate that microbially mediated sulfate reduction (MSR) is required. The $\Delta^{33}S$–$\delta^{34}S$ systematics of Hole U1301B basalts are consistent with open system alteration at high water/rock ratios (Ono et al., 2012), as was previously inferred from studies of the oxidative alteration signatures of upper crustal basalts combined with thermal constraints (Bach and Edwards, 2003). If MSR occurred at the current basement temperature of 65 °C, it can only explain about half of the Hole U1301B data (Ono et al., 2012). The other data are consistent with MSR at lower temperatures, down to 2 °C, indicating that it occurred early in the history of the site, prior to burial by sediment. This is consistent with cooler (3–50 °C) past basement fluid temperatures recorded by carbonate veins (Coggon et al., 2004). Alternatively, a few data are also consistent with derivation of sulfide from reactions in the sediment, which would require fluid flow from the sediment along focused zones in the basement.

The samples analyzed here include four background-halo sample pairs for which the S-isotope systematics were previously determined (Ono et al., 2012). The $\Delta^{33}S$–$\delta^{34}S$ data of U1301B 14R-1 65 (background, halo and pyrite front) indicate that the sulfides formed as a result of low temperature (2 °C) MSR, and are associated with significant Tl enrichment of the whole rock samples (up to 1500 ng/g; Table 1). High Tl concentrations (~100–260 ng/g) in the background portions of samples U1301B 25R-1 123, 32R-3 50 and 36R-1 53 are associated with MSR at warmer temperatures (~65 °C) consistent with modern basement conditions. These data indicate that Tl-uptake can be microbially mediated, and that Tl uptake may have begun prior to sedimentation of crust, and is still ongoing.

Given the observed association between Tl-uptake and secondary sulfide formation, the S-cycling in the ocean crust by sulfate reducing microbes is at least indirectly responsible for the uptake of Tl – a toxic heavy metal. Thallium uptake by the ocean crust may be analogous to processes being developed for the bioremediation of the anthropogenic releases of heavy metals to the environment via acid mine drainage (e.g., Pb, As, Cd, Cr, Co, Cu and

Zn) that use sulfate reducing bacteria to produce H_2S, which removes the metals from solution as metal sulfides (Sheoran et al., 2010).

7. CONCLUSIONS

Hydrothermal circulation is a key component of global biogeochemical cycles. Consequently reliable estimates of the hydrothermal fluid fluxes and associated chemical fluxes are important. Thallium is a potentially useful tracer of both high temperature axial and low temperature ridge flank hydrothermal circulation, given the distinct behavior of the Tl-isotopic system in the two hydrothermal regimes (Nielsen et al., 2006b). In this study, we investigated the mineralogical controls on Tl-uptake during hydrothermal alteration of the ocean crust, to improve our understanding of the conditions and timing of Tl-uptake, and assess the implications for hydrothermal fluid fluxes determined from mass balance of the ocean crust Tl-budget.

A compilation of published analyses of dredged MORB samples indicates that there is an association between Tl and alkali element uptake during seafloor weathering of basalt. However, given the lack of a clear relationship between the Tl and K contents of the seafloor weathered basalts, we conclude that the uptake of Tl and the alkali elements may not fully coupled but could involve, at least in part, different processes and/or mineral phases.

The Tl concentrations of upper crustal basalts from Holes U1301B, 504B and 896A correlate with S contents, indicating that Tl is incorporated into secondary sulfides. This hypothesis could be confirmed in future studies by in-situ measurements of Tl concentrations in sulfide and alkali-rich silicates. There is a clear depth limit to significant Tl-uptake in Hole 504B, as there are no samples with Tl concentrations that exceed the range of fresh MORB glass (1–30 ng/g; (Jenner and O'Neill, 2012)) below 210 meters sub-basement, despite net gains in S. This depth limit corresponds to the transition between the upper and lower alteration zones in Hole 504B. Thallium uptake during hydrothermal alteration of the ocean crust requires a Tl-bearing fluid and local conditions that favor the formation of secondary sulfide to provide a Tl-sink. Given evidence that secondary sulfides in the ocean crust form as a result of microbial sulfate reduction (Rouxel et al., 2008; Alt and Shanks, 2011; Ono et al., 2012; Lever et al., 2013), the microbial action is at least indirectly responsible for the uptake of Tl. In Hole U1301B, Tl is associated with sulfides that formed as a result of microbial sulfate reduction at temperatures between 2 and 65 °C (Ono et al., 2012).

Hydrothermal systems evolve with space and time as the crust spreads off axis and the thermal, chemical and hydrological conditions change. In general, upper crustal hydrothermal systems evolve from conditions with open circulation of oxidizing seawater to a more reducing regime that favors sulfide formation as the flow becomes more restricted (Alt et al., 1996a). Thallium uptake occurs in 'restricted' reducing environments; within the host rocks away from fluid flow pathways (cracks) during open system circulation and pervasively throughout the system as it evolves to a more restricted fluid flow regime. Estimates of the ridge flank hydrothermal fluid flux based on the Tl-isotope mass balance should therefore reflect fluid flow through both the 'open' and 'restricted' ridge flank systems.

ACKNOWLEDGEMENTS

The authors thank Barry Coles, Katharina Kreissig, Rasmus Andreasen and the other members of the MAGIC team for their help in keeping the mass spec and clean lab functioning. This research was supported by NERC Grant NE/E005616/1 to M.R., D.A.H.T. and R.M.C. and UK–IODP 301 post-cruise award NE/C513242/1 to R.M.C. and D.A.H.T.

APPENDIX A. SUPPLEMENTARY DATA

Supplementary data associated with this article can be found, in the online version, at http://dx.doi.org/10.1016/j.gca.2014.09.001.

REFERENCES

Albuquerque C. A. R., Muysson J. R. and Shaw D. M. (1972) Thallium in basalts and related rocks. *Chem. Geol.* **10**, 41–58.

Alt J. C. (1995) Subseafloor processes in mid-ocean ridge hydrothermal systems. In *Seafloor Hydrothermal Systems: Physical, Chemical, Biological and Geological Interactions within Hydrothermal Systems: Geophysical Monograph 91* (eds. S. E. Humphris, R. Zierenberg, L. Mullineaux and R. Thomson). American Geophysical Union, Washington, DC, pp. 85–114.

Alt J. C. (2004) Alteration of the upper oceanic crust: mineralogy, chemistry, and processes. In *Hydrogeology of the Oceanic Lithosphere* (eds. E. Davis and H. Elderfield). Cambridge University Press, pp. 456–488.

Alt J. C. and Shanks W. C. (2011) Microbial sulfate reduction and the sulfur budget for a complete section of altered oceanic basalts, IODP Hole 1256D (Eastern Pacific). *Earth Planet. Sci. Lett.* **310**, 73–83.

Alt J. C. and Teagle D. A. H. (2003) Hydrothermal alteration of upper oceanic crust formed at a fast-spreading ridge: mineral, chemical, and isotopic evidence from ODP Site 801. *Chem. Geol.* **201**, 191–211.

Alt J. C., Honnorez J., Laverne C. and Emmermann R. (1986) Hydrothermal alteration of a 1km section through the upper oceanic crust, Deep Sea Drilling Project Hole 504B: mineralogy, chemistry and evolution of seawater–basalt interactions. *J. Geophys. Res.* **91**, 10309–10335.

Alt J. C., Teagle D. A. H., Laverne C., Vanko D. A., Bach W., Honnorez J., Becker K., Ayadi M. and Pezard P. A. (1996a) Ridge flank alteration of upper ocean crust in the eastern Pacific: synthesis of results for volcanic rocks of Holes 504B and 896A. *Proc. ODP, Sci. Res.* **148**, 435–450.

Alt J. C., Laverne C., Vanko D. A., Tartarotti P., Teagle D. A. H., Bach W., Zuleger E., Erzinger J., Honnorez J., Pezard P. A., Becker K., Salisbury M. H. and Wilkens R. H. (1996b) Hydrothermal alteration of a section of upper oceanic crust in the Eastern Equatorial Pacific: a synthesis of results from site 504 (DSDP legs 69, 70 and 83, and ODP legs 111, 137, 140 and 148). In *Proceedings of the Ocean Drilling Program, Scientific Results, 148* (eds. J. C. Alt, H. Kinoshita, L. B. Stokking and P. J. Michael). pp. 417–434.

Bach W. and Edwards K. J. (2003) Iron and sulfide oxidation within the basaltic ocean crust: implications for chemolithoautotrophic microbial biomass production. *Geochim. Cosmochim. Acta* **67**, 3871–3887.

Bach W., Peucker-Ehrenbrink B., Hart S. R. and Blusztajn J. (2003) Geochemistry of hydrothermally altered oceanic crust: DSDP/ODP Hole 504B – implications for seawater-crust exchange budgets and Sr- and Pb-isotopic evolution of the mantle. *Geochem. Geophys. Geosyst.* **4**. http://dx.doi.org/10.1029/2002GC000419.

Baker R. G. A., Rehkamper M., Hinkley T. K., Nielsen S. G. and Toutain J. P. (2009) Investigation of thallium fluxes from subaerial volcanism—implications for the present and past mass balance of thallium in the oceans. *Geochim. Cosmochim. Acta* **73**, 6340–6359.

Baker R. G. A., Rehkamper M., Ihlenfeld C., Oates C. J. and Coggon R. (2010) Thallium isotope variations in an ore-bearing continental igneous setting: Collahuasi Formation, northern Chile. *Geochim. Cosmochim. Acta* **74**, 4405–4416.

Becker K. and Fisher A. (2000) Permeability of upper oceanic basement on the eastern flank of the Endeavor Ridge determined with drill-string packer experiments. *J. Geophys. Res.* **105**, 897–912.

Bickle M. J. and Teagle D. A. H. (1992) Strontium alteration in the Troodos ophiolite: implications for fluid fluxes and geochemical transport in mid-ocean ridge hydrothermal systems. *Earth Planet. Sci. Lett.* **113**, 219–237.

Butterfield D. A., Nelson B. K., Wheat C. G., Mottl M. J. and Roe K. K. (2001) Evidence for basaltic Sr in midocean ridge-flank hydrothermal systems and implications for the global oceanic Sr isotope balance. *Geochim. Cosmochim. Acta* **65**, 4141–4153.

Coggon R. M., Teagle D. A. H., Cooper M. J. and Vanko D. A. (2004) Linking basement carbonate vein compositions to porewater geochemistry across the eastern flank of the Juan de Fuca Ridge, ODP Leg 168. *Earth Planet. Sci. Lett.* **219**, 111–128.

Cowen J. P., Giovannoni S. J., Kenig F., Johnson H. P., Butterfield D., Rappé M. S., Hutnak M. and Lam P. (2003) Fluids from aging ocean crust that support microbial life. *Science* **299**, 120–123.

Davis E. E., Chapman D. S., Mottl M. J., Bentkowski W. J., Dadey K., Forster C., Harris R., Nagihara K., Rohr K., Wheat G. and Whiticar M. J. (1992) Flankflux: an experiment to study the nature of hydrothermal circulation in young ocean crust. *Can. J. Earth Sci.* **29**, 925–952.

Davis E. E., Fisher A. T., Firth J. V. and The ODP Leg 168 Shipboard Party. (1997) *Proceedings of the Integrated Ocean Drilling Program*, **168**. Ocean Drilling Program, College Station, TX.

Elderfield H., Wheat C. G., Mottl M. J., Monnin C. and Spiro B. (1999) Fluid and geochemical transport through oceanic crust: a transect across the eastern flank of the Juan de Fuca Ridge. *Earth Planet. Sci. Lett.* **172**, 151–165.

Fisher A. T. (2003) Geophysical constraints on hydrothermal circulation: observations and models. In *Energy and Mass Transfer in Marine Hydrothermal Systems* (eds. P. E. Halbech, V. Tunnicliffe and J. R. Hein). Dahlem University Press, Berlin, pp. 29–52.

Fisher A., Davis E. E. and Escutia C. (2000) *Proc. ODP Sci. Res.* **168**. Ocean Drilling Program, College Station, TX.

Fisher A. T., Davis E. E., Hutnak M., Spiess V., Zuhlsdorff L., Cherkaoui A., Christiansen L., Edwards K., Macdonald R., Villinger H., Mottl M. J., Wheat C. G. and Becker K. (2003) Hydrothermal recharge and discharge across 50 km guided by seamounts on a young ridge flank. *Nature* **421**, 618–621.

Fisher A., Urabe T., Klaus A. and The Expedition 301 Scientists. (2005) *Proceedings of the Integrated Ocean Drilling Program*, **301**. Integrated Ocean Drilling Program Management International, Inc., College Station, TX.

Fisher A. T., Tsuji T., Petronotis K. and The Expedition 327 Scientists. (2011) *Proceedings of the Integrated Ocean Drilling Program*, **327**. Integrated Ocean Drilling Program Management International, Inc., Tokyo.

Goldschmidt V. M. (1954) *Geochemistry*. Oxford University Press, Oxford.

Hart S. R. (1969) K, Rb, Cs contents and K/Rb, K/Cs ratios of fresh and altered submarine basalts. *Earth Planet. Sci. Lett.* **6**, 295–303.

Heinrichs H., Schulz-Dobrick B. and Wedepohl K. H. (1980) Terrestrial geochemistry of Cd, Bi, Tl, Pb, Zn, and Rb. *Geochim. Cosmochim. Acta* **44**, 1519–1533.

Hubberten H.-W., Emmermann R. and Puchelt H. (1983) Geochemistry of basalts from Costa Rica Rift Sites 504 and 505 (Deep Sea Drilling Project Legs 69 and 70). In *Init. Repts. DSDP* (eds. J. R. Cann, M. G. Langseth, J. Honnorez, R. P. Von Herzen and S. M. White). U.S. Govt. Printing Office, Washington, pp. 791–803.

Hunter A. G., Kempton P. D. and Greenwood P. (1999) Low-temperature fluid–rock interaction – an isotopic and mineralogical perspective of upper crustal evolution, eastern flank of the Juan de Fuca Ridge (JdFR), ODP Leg 168. *Chem. Geol.* **155**, 3–28.

Jenner F. E. and O'Neill H. S. C. (2012) Analysis of 60 elements in 616 ocean floor basaltic glasses. *Geochem. Geophys. Geosyst.* **13**.

Jochum K. P. and Verma S. P. (1996) Extreme enrichment of Sb, Tl and other trace elements in altered MORB. *Chem. Geol.* **130**, 289–299.

Kiseeva E. S. and Wood B. J. (2013) A simple model for chalcophile element partitioning between sulphide and silicate liquids with geochemical applications. *Earth Planet. Sci. Lett.* **383**, 68–81.

Lear C. H., Rosenthal Y. and Slowey N. (2002) Benthic foraminiferal Mg/Ca-paleothermometry: a revised core-top calibration. *Geochim. Cosmochim. Acta* **66**, 3375–3387.

Lever M. A., Rouxel O., Alt J. C., Shimizu N., Ono S., Coggon R. M., Shanks, III, W. C., Lapham L., Elvert M., Prieto-Mollar X., Hinrichs K.-U., Inagaki F. and Teske A. (2013) Evidence for microbial carbon and sulfur cycling in deeply buried ridge flank basalt. *Science* **339**, 1305–1308.

Marescotti P., Vanko D. A. and Cabella R. (2000) From oxidising to reducing alteration: mineralogical variations in pillow basalts from the east flank, Juan de Fuca Ridge. In *Proc. ODP: Sci. Res.* (eds. A. Fisher, E. E. Davis and C. Escutia). Ocean Drilling Program, College Station, TX. pp. 119–136.

McGoldrick P. J., Keays R. R. and Scott B. B. (1979) Thallium: a sensitive indicator of rock/seawater interaction and of sulfur saturation of silicate melts. *Geochim. Cosmochim. Acta* **43**, 1303–1311.

Mottl M. J. (2003) Partitioning of energy and mass fluxes between mid-ocean axes and flanks at high and low temperature. In *Energy and Mass Transfer in Marine Hydrothermal Systems* (eds. P. E. Halbech, V. Tunnicliffe and J. R. Hein). Dahlem University Press, pp. 271–286.

Mottl M. J. and Wheat C. G. (1994) Hydrothermal circulation through mid-ocean ridge flanks – fluxes of heat and magnesium. *Geochim. Cosmochim. Acta* **58**, 2225–2237.

Nielsen S. G., Rehkämper M., Porcelli D., Andersson P., Halliday A. N., Swarzenski P. W., Latkoczy C. and Günther D. (2005) Thallium isotope composition of the upper continental crust and rivers—an investigation of the continental sources of dissolved marine thallium. *Geochim. Cosmochim. Acta* **19**, 2007–2019.

Nielsen S. G., Rehkämper M., Norman M. D., Halliday A. N. and Harrison D. (2006a) Thallium isotopic evidence for ferromanganese sediments in the mantle source of Hawaiian basalts. *Nature* **439**, 314–317.

Nielsen S. G., Rehkämper M., Teagle D. A. H., Butterfield D. A., Alt J. C. and Halliday A. N. (2006b) Hydrothermal fluid fluxes calculated from the isotopic mass balance of thallium in the ocean crust. *Earth Planet. Sci. Lett.* **251**, 120–133.

Nielsen S. G., Rehkämper M., Brandon A. D., Norman M. D., Turner S. and O'Reilly S. Y. (2007) Thallium isotopes in Iceland and Azores lavas – implication for the role of altered crust and mantle geochemistry. *Earth Planet. Sci. Lett.* **264**, 332–345.

Nielsen S. G., Mar-Gerrison S., Gannoun A., LaRowe D., Klemm V., Halliday A. N., Burton K. W. and Hein J. R. (2009) Thallium isotope evidence for a permanent increase in marine organic carbon export in the early Eocene. *Earth Planet. Sci. Lett.* **278**, 297–307.

Nielsen S. G., Wasylenki L. E., Rehkämper M., Peacock C. L., Xue Z. and Moon E. M. (2013) Towards an understanding of thallium isotope fractionation during adsorption to manganese oxides. *Geochim. Cosmochim. Acta* **117**, 252–256.

Ono S., Keller N. S., Rouxel O. and Alt J. C. (2012) Sulfur-33 constraints on the origin of secondary pyrite in altered oceanic basement. *Geochim. Cosmochim. Acta* **87**, 323–340.

Peacock C. L. and Moon E. M. (2012) Oxidative scavenging of thallium by birnessite: explanation for thallium enrichment and stable isotope fractionation in marine ferromanganese precipitates. *Geochim. Cosmochim. Acta* **84**, 297–313.

Prokoph A. and Veizer J. (1999) Trends, cycles and nonstationarities in isotope signals of phanerozoic seawater. *Chem. Geol.* **161**, 225–240.

Prytulak J., Nielsen S. G., Plank T., Barker M. and Elliott T. (2013) Assessing the utility of thallium and thallium isotopes for tracing subduction zone inputs to the Mariana arc. *Chem. Geol.* **345**, 139–149.

Rehkämper M. and Nielsen S. G. (2004) The mass balance of dissolved thallium in the oceans. *Mar. Chem.* **85**, 125–139.

Rehkämper M., Frank M., Hein J. R., Porcelli D., Halliday A., Ingri J. and Liebetrau V. (2002) Thallium isotope variations in seawater and hydrogenetic, diagenetic, and hydrothermal ferromanganese deposits. *Earth Planet. Sci. Lett.* **197**, 65–81.

Rice C. A., Tuttle M. L. and Reynolds R. L. (1993) The analysis of forms of sulfur in ancient sediments and sedimentary rocks — comments and cautions. *Chem. Geol.* **107**, 83–95.

Rouxel O., Ono S., Alt J. C., Jumble D. and Ludden J. (2008) Sulfur isotope evidence for microbial sulfate reduction in altered oceanic basalts at ODP Site 801. *Earth Planet. Sci. Lett.* **268**, 110–123.

Shannon R. D. (1976) Revised effective ionic radii and systematic studies of interatomic distances in halides and chalcogenides. *Acta Crystallogr.* **A32**, 751–767.

Shaw D. M. (1952) The geochemistry of thallium. *Geochim. Cosmochim. Acta* **2**, 118–154.

Sheoran A. S., Sheoran V. and Choudhary R. P. (2010) Bioremediation of acid-rock drainage by sulphate-reducing prokaryotes: a review. *Miner. Eng.* **23**, 1073–1100.

Stein C. A. and Stein S. (1994) Constraints on hydrothermal heat-flux through the oceanic lithosphere from global heat-flow. *J. Geophys. Res.* **99**, 3081–3095.

Su X., Baumann K.-H. and Thiede J. (2000) Calcareous nannofossils from Leg 168: biochronology and diagenesis. In *Proc. ODP: Sci. Res.* (eds. A. Fisher, E. E. Davis and C. Escutia). Ocean Drilling Program, College Station, TX. pp. 39–49.

Teagle D. A. H., Alt J. C., Bach W., Halliday A. N. and Erzinger J. (1996) Alteration of upper ocean crust in a ridge-flank hydrothermal upflow zone: mineral, chemical, and isotopic constraints from Hole 896A. *Proc. ODP, Sci. Res.* **148**, 119–150.

Thode H. G., Monster J. and Dunford h. B. (1961) Sulfur isotope geochemistry. *Geochim. Cosmochim. Acta* **25**, 159–174.

Underwood M. B., Hoke K. D., Fisher A. T., Davis E. E., Giambalvo E., Zühlsdorff L. and Spinelli G. A. (2005) Provenance, stratigraphic architecture, and hydrogeologic influence of turbidites on the mid-ocean ridge flank of northwestern Cascadia Basin, Pacific Ocean. *J. Sediment. Res.* **75**, 149–164.

Vance D., Teagle D. A. H. and Foster G. L. (2009) Variable quaternary chemical weathering fluxes and imbalances in marine geochemical budgets. *Nature* **458**, 493–496.

Veizer J., Ala D., Azmy K., Bruckschen P., Buhl P., Bruhn F., Carden G. A. F., Diener A., Ebneth S., Godderis Y., Jasper T., Korte C., Pawellek F., Podlaha O. G. and Strauss H. (1999) $^{87}Sr/^{86}Sr$, $\delta^{13}C$ and $\delta^{18}O$ evolution of Phanerozoic seawater. *Chem. Geol.* **161**, 59–88.

Wedepohl K. H. (1974) *Handbook of Geochemistry*. Springer, Berlin.

Wheat C. G. and Mottl M. J. (2000) Compositions of pore and spring waters from Baby Bare: global implications of geochemical fluxes from a ridge flank hydrothermal system. *Geochim. Cosmochim. Acta* **64**, 629–642.

Wheat C. G., Elderfield H., Mottl M. J. and Monnin C. (2000) Chemical composition of basement fluids within an oceanic ridge flank: implications for along-strike and across-strike hydrothermal circulation. *J. Geophys. Res.* **105**, 13437–13447.

Wheat C. G., Mottl M. J. and Rudnicki M. (2002) Trace element and REE composition of a low-temperature ridge-flank hydrothermal spring. *Geochim. Cosmochim. Acta* **66**, 3693–3705.

Wheat C. G., Jannasch H. W., Kastner M., Plant J. N., DeCarlo E. H. and Lebon G. (2004) Venting formation fluids from deep-sea boreholes in a ridge flank setting: ODP Sites 1025 and 1026. *Geochem. Geophys. Geosyst.* **5**, Q08007. http://dx.doi.org/10.01029/02004GC000710.

Wheat C. G., Jannasch H. W., Fisher A. T., Becker K., Sharkey J. and Hulme S. (2011) Subseafloor seawater-basalt-microbe reactions: continuous sampling of borehole fluids in a ridge flank environment. *Geochem. Geophys. Geosyst.* **11**.

Wheat C. G., Hulme S. M., Fisher A. T., Orcutt B. N. and Becker K. (2013) Seawater recharge into oceanic crust: IODP Exp 327 Site U1363 Grizzly Bare outcrop. **14**.

Wood B. J., Nielsen S. G., Rehkämper M. and Halliday A. N. (2008) The effects of core formation on the Pb- and Tl-isotopic composition of the silicate Earth. *Earth Planet. Sci. Lett.* **269**, 326–336.

Xiao T., Jayanta G. and Boyle D. (2004) High thallium content in rocks associated with Au–As–Hg–Tl and coal mineralization and its adverse environmental potential in SW Guizhou, China. *Geochem.: Explor. Environ. Anal.* **4**, 243–252.

Zachos J., Pagani M., Sloan L., Thomas E. and Billups K. (2001) Trends, rhythms and aberrations in global climate, 65 Ma to present. *Science* **292**, 686–693.

Associate editor: Wolfgang Bach